applied sciences

MDPI

Article

Bearing Characteristics and Ground Deformation Computation of Recyclable Steel-Pipe Piles during Pit Excavation

Jian Lu [1], Yanlin Li [2,*] and Aijun Yao [2]

[1] Road Safety Research Center, Research Institute of Highway Ministry of Transport, Beijing 100088, China; lj_beyond@sina.com
[2] Key Laboratory of Urban Security and Disaster Engineering, Ministry of Education, Beijing University of Technology, Beijing 100124, China; yaj@bjut.edu.cn
* Correspondence: liyanlin955@emails.bjut.edu.cn

Abstract: In the context of increasing environmental awareness and the demand for sustainable construction practices, the use of recyclable materials in civil engineering projects has gained significant attention. This study focuses on the bearing characteristics and deformation behavior of recyclable steel-pipe piles during the excavation of foundation pits. Field experiments and numerical simulations were conducted to comprehensively analyze the stress characteristics and surface settlement patterns behind the piles. The results reveal critical insights into the interaction between the steel-pipe piles and the surrounding soil, providing a detailed understanding of the stress distribution and deformation mechanisms. An empirical method for calculating the surface settlement value, induced by foundation pit excavation under the support of steel-pipe slope protection piles, has been proposed. This method improves the accuracy of settlement predictions and enhances the reliability of foundation pit design.

Keywords: recoverable steel-pipe piles; supporting structure; field test; pile strain; ground surface settlement

Citation: Lu, J.; Li, Y.; Yao, A. Bearing Characteristics and Ground Deformation Computation of Recyclable Steel-Pipe Piles during Pit Excavation. *Appl. Sci.* **2024**, *14*, 5727. https://doi.org/10.3390/app14135727

Academic Editor: Tiago Miranda

Received: 1 June 2024
Revised: 27 June 2024
Accepted: 29 June 2024
Published: 30 June 2024

1. Introduction

Urbanization in China has been accelerating in recent years, leading to an increase in the number of buildings and corresponding foundation pit engineering projects. Many underground engineering constructions have driven the development of foundation pit support systems. Traditional support structures in foundation pit engineering primarily include double-row piles [1], pile-anchor bolt support [2–4], and underground diaphragm walls. However, these conventional methods have significant drawbacks, such as non-recoverable components, material waste, and high construction costs.

With advancements in construction technologies, there is a growing emphasis on cost control and environmental protection in underground construction. This has led to a focus on technologies for recoverable foundation pit-supporting structures [5]. These recoverable structures are designed with the characteristics of foundation pit projects in mind, emphasizing reusability and sustainability. They offer several advantages, including high construction quality, convenient construction methods, and the ability to recover and reuse components.

Researchers have conducted extensive studies on performance and deformation behavior of recoverable foundation pit-supporting structures. These studies have primarily focused on the bearing capacity, construction technology, and uplift resistance of recoverable anchor cables through numerical simulations and experimental methods [6–8]. Pan [9] studied the construction process of an underground granary and identified the deformation characteristics of recyclable support structures. Research on steel-pipe piles has concentrated on two main aspects: micro and large-diameter steel-pipe piles. Existing studies

have examined the applicability of micro steel-pipe piles in foundation pit support and reinforcement projects through model tests and field tests, revealing their action mechanisms and stress-bearing deformation patterns [10]. For large-diameter open-mouth steel-pipe piles, Zhang [11] used numerical simulation to study their load-bearing and settlement characteristics. Field tests have provided insights into the frictional resistance distribution along the pile body and the soil parameter values adjacent to the piles through combined field and numerical methods [12,13]. Recent studies have extensively explored the application of micro steel-pipe piles in foundation pit support, while research on large-diameter steel-pipe piles has highlighted their stress-bearing and operational effectiveness when used as foundation piles.

The excavation process of foundation pits inevitably disturbs the surrounding soil, causing deformation in both the supporting structures and the affected soil. Existing studies have focused on the settlement behavior of support structures and soil during the excavation process, particularly within the two-dimensional influence area of settlement [14–17]. Additionally, soil settlement laws have been studied in the context of foundation pit dewatering [18–20]. In practical scenarios, foundation pits exhibit three-dimensional deformation. Many researchers have studied them through multiple methods [21–26]. The settlement of soil behind pit walls varies between the long and short sides due to spatial effects. Ou [27] analyzed measured data to determine the settlement laws of soil and the deformation of supporting structures under spatial effects based on statistical analysis of measured data from the excavation of thirty metro stations in Nanjing. Li [28] divided the soil behind foundation pit walls into two areas: Area A, unaffected by spatial effects, and Area B, affected by spatial effects. Li proposed ground surface settlement patterns for different influence areas, but these patterns consist of three broken lines that differ from the actual ground surface settlement curves.

In summary, few studies have been conducted on the application of recoverable large-diameter steel-pipe piles in foundation pit support processes. Therefore, it is crucial to study the mechanical performance of these steel-pipe piles in such applications. This study employs field tests and finite element analysis methods to investigate the performance of large-diameter recoverable steel-pipe piles. It examines the deformation patterns of the piles during the support process and the ground surface settlement caused by excavation. Furthermore, a mathematical formula for ground surface settlement is proposed, providing valuable insights for application of recoverable steel-pipe piles in foundation pit engineering.

2. Methodology

2.1. Field Test

To study the supporting effect and deformation laws of recoverable large-diameter steel-pipe piles during the foundation pit excavation process, a field test was conducted. The test site, which is flat and broad, is located in the northwest of Beijing. From top to bottom, strata soil textures in this site are ① miscellaneous fill, ② clayey silt, ③ sandy silt, ④ sand, and ⑤ silty clay, according to Figure 1b.

The excavation depth of the test foundation pit is 6.5 m. Considering the field soil textures and site conditions, slopes are reserved at the three sides of the test foundation pit. One site is supported by four recoverable steel-pipe piles, and their length is 12.5 m. To reduce the resistance between recoverable steel-pipe piles and surrounding materials during the steel-pipe pile recovery process, the steel-pipe pile body is designed with a conical shape. Moreover, the top diameter and bottom diameter of the steel-pipe piles are 630 and 530 mm, respectively. The wall thickness of the steel-pipe pile body is 10 mm. Considering the insufficient pile body stiffness during the uplift process, the pile body was thickened (thickness: 30 mm) within the 1 m range of the pipe top and welded with a stiffening rib. For the convenience of hanging, two lifting holes of a diameter of 30 mm are drilled into the stiffening rib. Figure 2 depicts the recoverable steel-pipe pile structure.

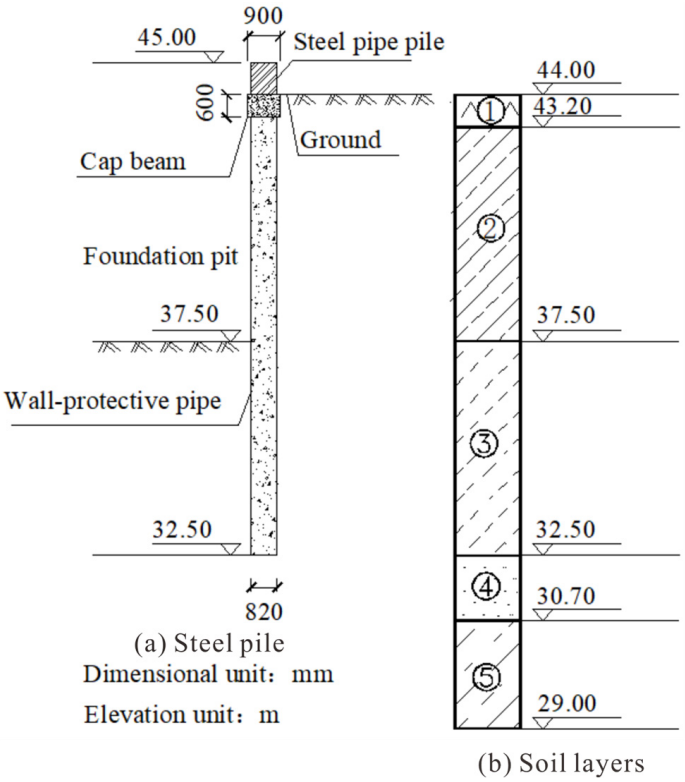

Figure 1. Cross-sectional graph of the supporting structure. (**a**) Steel pipe; (**b**) soil layers.

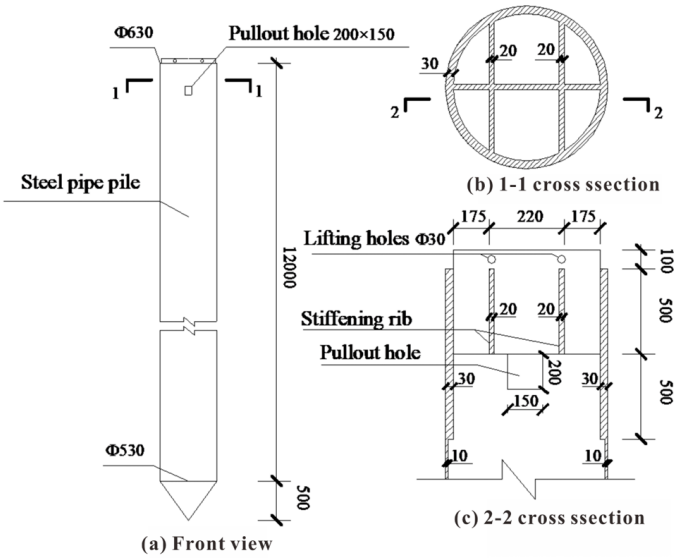

Figure 2. Recoverable steel-pipe pile structure. (**a**) Front view; (**b**) 1–1 cross section; (**c**) 2–2 cross section.

A reverse circulation drill is used for the steel-pipe pile hole drilling. The wall of the hole is protected by the slurry. To prevent the collapse of the pile holes before the steel-pipe piles are inserted, a wall-protective pipe is set inside the pile holes. The wall-protective pipe texture selected in this test is C25 concrete. Its inner diameter is 700 mm, the wall thickness is 60 mm, and the length of each segment of the concrete wall-protective pipe is 2 m. Figure 3 demonstrates the concrete wall-protective pipe.

Figure 3. Concrete wall-protective pipe.

The main monitoring items in this test are pile body strain, ground surface settlement at the rear side of the supporting structure, and the horizontal displacement of the pile top.

(1) Layout of the strain gauge on the pile body and monitoring device

To explore the mechanical performance of the steel-pipe piles during the foundation pit excavation process, 10 strain monitoring points were arranged at the front and rear sides of each steel-pipe pile. A resistance-type strain gauge was pasted on each strain monitoring point. Figure 4 displays the strain gauge. The pile body strain data were collected using a DH3816N static strain testing system, as exhibited in Figure 5. Figures 6 and 7 illustrate the layout of the pile body strain gauge.

(2) Layout of the monitoring points of pile top displacement and monitoring device

The horizontal displacement of the pile top was collected using a guyed displacement sensor (range: 0–100 mm, accuracy: 0.01 mm) and a YT-1 absolute displacement acquisition meter during the test process, as presented in Figures 8 and 9, respectively.

Figure 4. Resistance-type strain gauge.

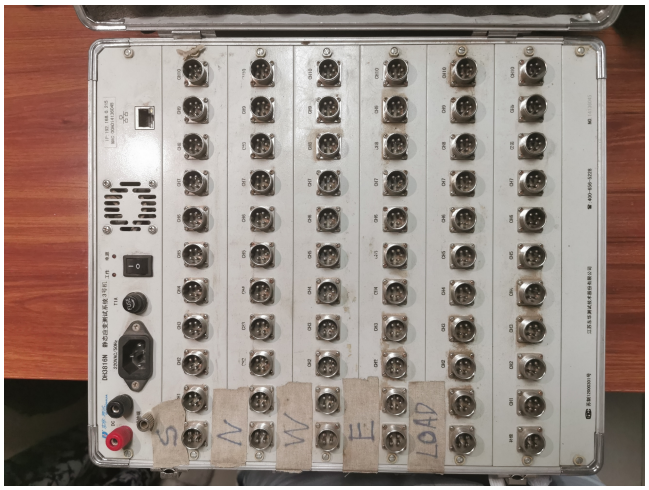

Figure 5. DH3816N static strain testing system.

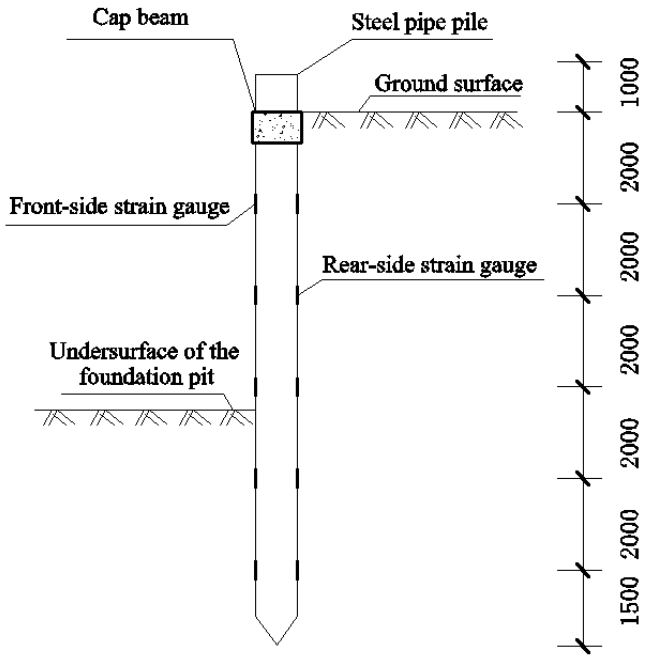

Figure 6. Layout of the strain gauges.

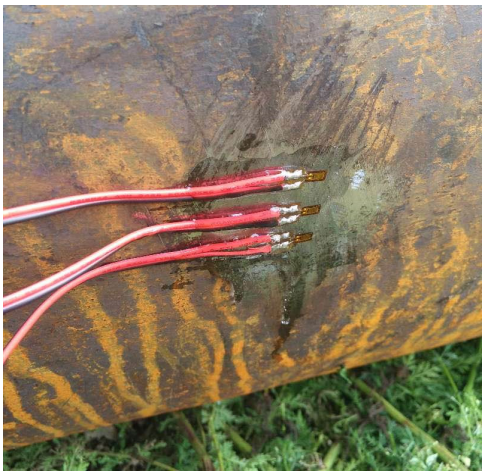

Figure 7. Strain gauge glueing.

Figure 8. Guyed displacement sensor.

Figure 9. YT-1 absolute displacement acquisition meter.

The displacement monitoring point was set at the position behind each steel-pipe pile, with an elevation of 44 m. The guyed displacement sensor was also fastened onto the fixed point beyond the influence area of the foundation pit excavation. In addition, the sensor was connected to the monitoring point of the horizontal displacement of the pile top using a steel-stranded wire. Moreover, the protective casing pipe was used to cover the external side. Figure 10 depicts the elevation of the monitoring points of the horizontal displacement of the pile top.

(3) Layout plan of the monitoring points of the ground surface settlement

Restricted by the test site conditions, three ground surface settlement monitoring lines were arranged on the ground at the rear side of the supporting structure. Each monitoring line had eight monitoring points. Figure 11 demonstrates the monitoring point layout. The monitoring data of the ground surface settlement at the rear side of the supporting structure were collected using an electronic-level Trimble DiNi03.

After arranging the strain gauges on the steel-pipe pile body, the pile was hung in the pile hole set with a wall-protective pipe. Cement paste filled the gap between the steel-pipe pile and wall-protective pipes. A cap beam was created after the cement paste hardened. Its dimensions (width $\times$ height) were 0.9 m $\times$ 0.6 m, and the concrete grade of the cap beam was C25. After the cap beam reached the design strength, the foundation pit was excavated, and the excavation depth was 6.5 m. The excavation was implemented in three steps. The excavation depth in the first and second step was 2 m, whereas that in the third

step was 2.5 m. Data of the monitoring points were acquired during the excavation process. Figure 12 exhibits the foundation pit excavation.

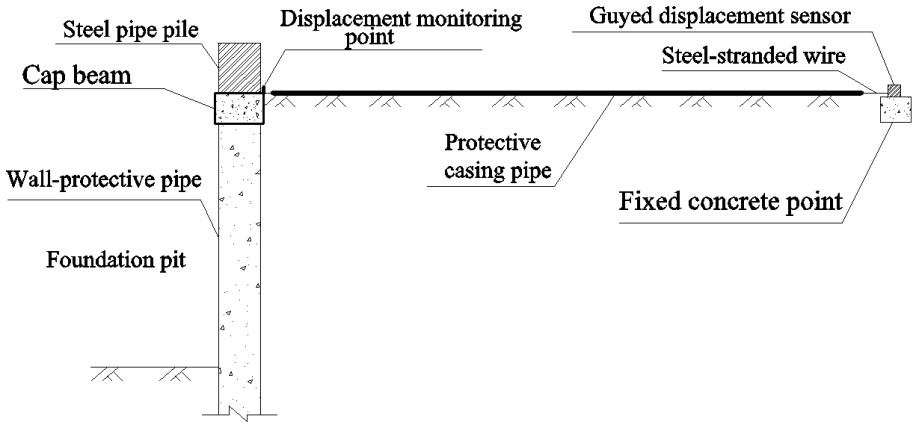

Figure 10. Elevation drawing of the monitoring points of the horizontal displacement of the pile top.

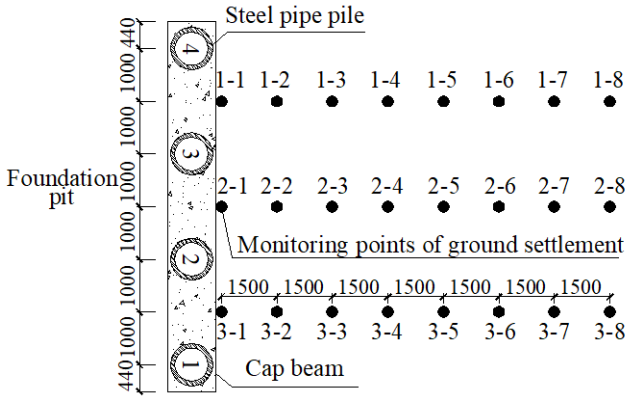

Figure 11. Monitoring point layout.

Figure 12. Excavation of the foundation pit.

2.2. Finite Element Analysis

To further explore the deformation laws of steel-pipe piles after the foundation pit excavation, finite element software Midas GTS-NX was used to conduct a numerical analysis and simulation of the foundation pit excavation process.

The soil is an isotropic medium in this calculation model and presented a stratified distribution in the horizontal direction. The influence of underground water was disregarded in the numerical analysis and calculation process. The hardening soil model can take into account the non-linear characteristics of the stress and strain of soil, and can reflect the complex stress path of soil during the excavation of a foundation pit [29,30]. Therefore, the modified Mohr–Coulomb constitutive model was used during the calculation process.

The dimension of the foundation pit excavation in the model was 40 m × 40 m (length × width), and the excavation depth was 6.5 m. A total of six times the excavation depth of the foundation pit was set in the horizontal direction of the soil outside the foundation pit, whereas 3.6 times the depth was set below the undersurface of the foundation pit. The calculation model dimension was 80 m × 80 m × 30 m (length × width × height). The numerical model is shown in Figure 13. The soil was simulated using solid elements, according to the geological survey report from the Beijing Institute of Geological Survey and Design. Table 1 displays the material mechanical parameters of the soil. The steel-pipe piles and cap beam were simulated using the beam elements. Table 2 lists the material mechanical parameters of the supporting structure according to the support structure design documents.

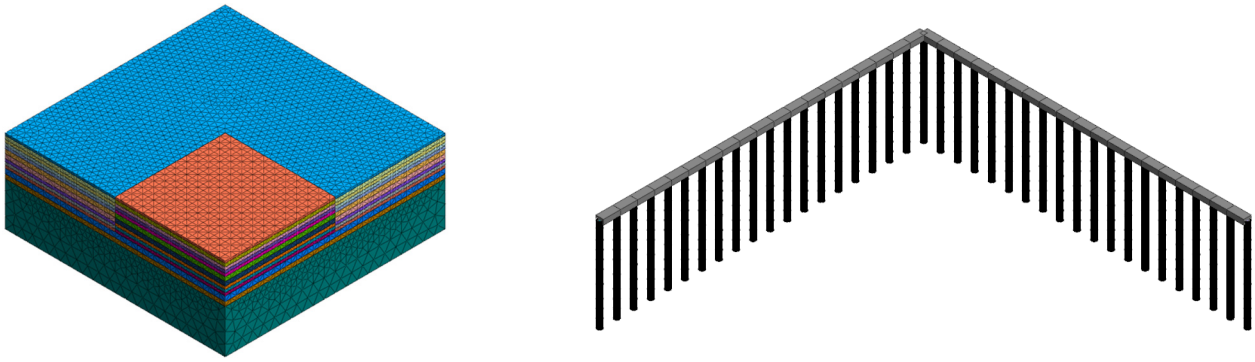

(**a**) (**b**)

Figure 13. Components of numerical model gridding. (**a**) Overall model gridding (**b**) Steel-pipe pile beam model.

Table 1. Material mechanical parameters of the soil.

Name	Thickness (m)	Poisson Ratio	Unit Weight (kN/m^3)	Cohesion (kPa)	Internal Friction Angle (°)	Compression Modulus (MPa)
Miscellaneous fill	0.8	0.35	16.5	0	8	5
Clayey silt	5.7	0.25	19.7	9	16	11
Sandy silt	4.5	0.26	19.9	14	18	14
Fine sand	1.8	0.27	19.5	0	30	30
Silty clay	17.2	0.26	20	20	22	26

Table 2. Material mechanical parameters of the supporting structure.

Name	Elastic Modulus (MPa)	Poisson Ratio	Unit Weight (kN/m^3)
Steel-pipe pile	206,000	0.3	78
Cap beam	28,361	0.25	25

During the numerical simulation of the foundation pit excavation under the supporting of the large-diameter steel-pipe piles, three steps were performed.

First, the soil grids of the model were activated. Then, the boundary constraint and soil load were applied to grids. Finally, the displacement was reset to 0.

Second, the piles and cap beams were constructed. Then, the displacement was also reset to 0.

Third, the foundation pit was excavated 3 times with excavation depths of 2, 2, and 2.5 m.

3. Results Analysis and Discussion

3.1. Pile Strain and Bending Moment

During the test process, the strain of the steel-pipe pile body was monitored through the resistance strain gauge pasted on the pile body. The strains of No. 2 pile body, measured three times after the foundation pit excavation was completed, were selected for the analysis, as displayed in Figures 14 and 15. A positive value of the pile body strains indicates that the monitoring point is under a tensile state, whereas a negative value indicates that the monitoring point is under a compressive state. The pile body experiences positive bending if its rear side is under a tensile force while its front side is under a compressive force. By contrast, the pile body withstands negative bending if its rear side is under a compressive force while its front side is under a tensile force.

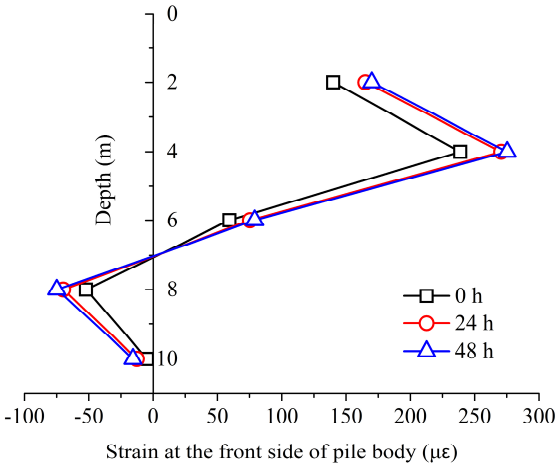

Figure 14. The strain at the front side of the pile body.

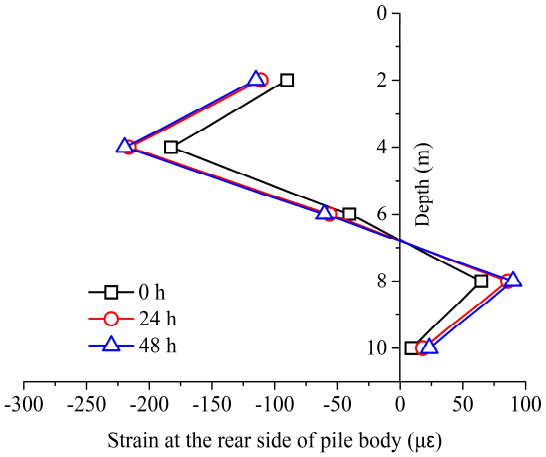

Figure 15. The strain at the rear side of the pile body.

Figure 14 presents that, after the foundation pit excavation, a strain change at the front side of the pile body gradually stabilized with time. The front side of the pile body above the undersurface of the foundation pit was mainly under the tensile state. The maximum tensile strain was 275 με, which occurred at 4 m below the ground surface. At the position below the undersurface of the foundation pit, the front side of the pile body was under the compressive state. The maximum compressive strain was −75 με, which occurred at 1.5 m below the undersurface of the foundation pit. Near the undersurface, zero-strain points appeared at the front side of the pile body. The strain value at the front side of the pile body was greater above the undersurface of the foundation pit than below.

Through an analysis of the rear-side strain of the pile body, the following conclusions were drawn. After completing the foundation pit excavation, the tensile region at the rear side of the pile body was mainly distributed below the undersurface of the foundation pit. However, the compressive region at the rear side of the pile body was mainly distributed above the undersurface of the pit. The maximum compressive strain at the rear side of the pile body occurred at 4 m below the ground surface, whereas the maximum tensile strain occurred at 1.5 m below the undersurface of the foundation pit. Zero strain at the rear side of the pile body occurred near the undersurface of the foundation pit. The strain value at the rear side of the pile body was smaller below the undersurface of the foundation pit than above.

Through a comparative analysis of the front-side and rear-side strains of No. 2 pile body, the front side was under the tensile state above the undersurface of the foundation pit, whereas its rear side was under the compressive state. The pile body experienced negative bending, and the maximum bending deformation of the pile body occurred at 0.62 H (H is the depth of the foundation pit excavation) below the ground surface. This result was due to the fact that the supporting structure underwent bending deformation toward the foundation pit under the action of a constraining effect of the cap beam and the active earth pressure behind the supporting structure. Below the undersurface of the foundation pit, the front side of the pile body was under the compressive state, whereas its rear side was under the tensile state. The pile body experienced positive bending, and its maximum bending deformation occurred at 0.23 H below the undersurface of the foundation pit. The front- side and rear-side strain curves of the pile body were relatively symmetrical.

According to the theory of elastic beam, the curvature of the pile body φ can be obtained using:

$$\varphi = \frac{1}{\rho} = \frac{\Delta\varepsilon}{h}, \quad (1)$$

where

ρ—curvature radius of the pile body (m);

$\Delta\varepsilon$—difference value of the strain between the two symmetrical sides of the cross-section pile body;

h—cross-section height of the pile body (m).

Then, the bending moment M of the pile body can be obtained as:

$$M = EI \times \varphi, \quad (2)$$

where

EI—flexural rigidity of the cross-section pile (kN·m^2).

The measured pile body strain was converted into a bending moment in accordance with Equations (1) and (2). Then, the result was compared to the pile-body bending moment calculated through finite element analysis after the excavation, as exhibited in Figure 16.

Figure 16 presents that, after the foundation pit excavation, the maximum negative bending moment of the pile body occurred at 4 m below the ground surface (at −129 kN·m). By contrast, the maximum positive bending moment occurred at 1.5 m below the undersurface of the foundation pit (at 51.9 kN·m in the finite element analysis result).

The analysis of the bending moment distribution laws of the pile body after the excavation revealed that the pile-body bending moment above the undersurface of the foundation pit had a negative value. Moreover, the maximum negative bending moment occurred at 0.62 H below the ground surface. Below the undersurface of the foundation pit, the bending moment of the pile-body was positive, and its maximum bending moment occurred at 0.23 H below the undersurface of the foundation pit. The pile-body stress-bearing deformation laws in the finite element analysis result agreed with the field test measured result. Therefore, the finite element analysis model was reasonable.

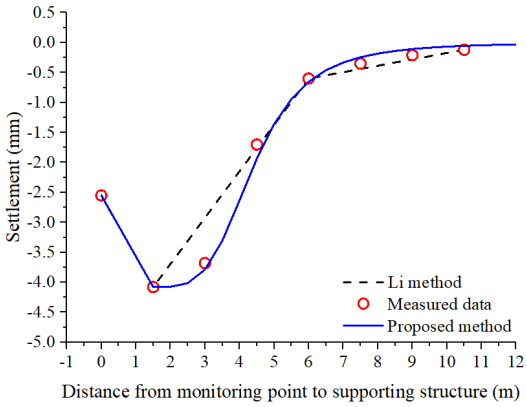

Figure 16. Comparison of the measured and finite element analysis bending moments of the pile body.

3.2. Cross-Section Strength Analysis of the Pile

To analyze the safety of the pile-body structure, Equation (3) was used to verify the calculation result of the cross-section normal stress [31].

$$\sigma = M_x/(\gamma \cdot W_x) \leq f, \tag{3}$$

where

σ—cross-sectional normal stress (MPa);
M_x—bending moment at the cross section around the x-axis (kN·m);
γ—cross-sectional plastic development coefficient;
W_x—net cross-sectional modulus of the x-axis (m^3);
f—design value of steel flexural strength (MPa).

The steel-pipe pile texture used in the test was Q235 steel. According to the design code for steel structures, the design value of steel flexural strength was 215 MPa. Moreover, the cross-sectional plastic development coefficient was 1.15. In the finite element analysis results, the maximum bending moment of the pile body was 129 kN·m. In accordance with Equation (3), the maximum cross-sectional normal stresses could be calculated as 44.9 MPa, which was within the permissible range of the design value of steel flexural strength. Therefore, upon completing the foundation pit excavation, the internal force of the steel-pipe pile structure was small, and the structure was safe.

3.3. Analysis of the Horizontal Displacement of the Pile Top

Figure 17 illustrates the change curves of the horizontal displacement of the pile top in the field test.

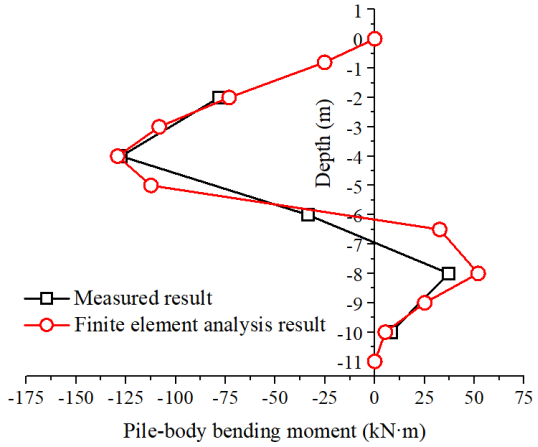

Figure 17. Change curves of the horizontal displacement of the pile top.

In this figure, the steel-pipe pile top experienced displacement towards the foundation pit during the excavation process. Then, the pile top reached the maximum displacement deformation (at 5.63 mm). The overall deformation was not large and was smaller than the alarm value (50 mm) stipulated in the technical code for the monitoring of building excavation engineering [31]; the supporting effect of steel-pipe piles was favorable. Pile-top displacement deformations were larger in piles No. 2 and 3 than in piles No. 1 and 4 because piles No. 1 and 4 were side piles. Furthermore, the embedding effect of the surrounding unexcavated soil for piles No. 1 and 4 reduced the pile-top displacement toward the foundation pit.

In addition, the pile-top displacement rate was low after completing the first step of the foundation pit excavation. In the first excavation step, the active earth pressure of the soil at the rear side of the supporting structure was not large. The pile body also experienced a small deformation under the constraining effect of the cap beam and such an active earth pressure. The active earth pressure and pile-top displacement gradually increased with the excavation depth.

3.4. Analysis of the Ground Surface Settlement

The curve of ground settlement monitoring line No. 1 after the foundation pit excavation was selected, as depicted in Figure 18.

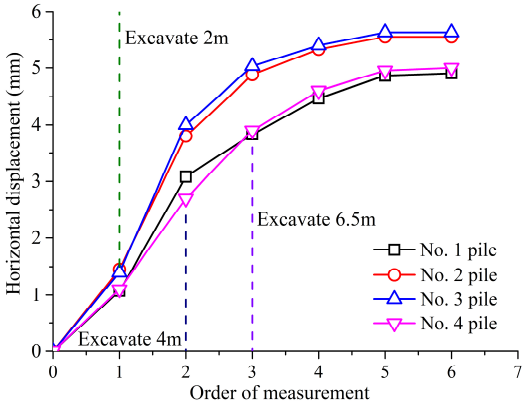

Figure 18. Settlement curve of the ground surface.

After completing the foundation pit excavation, and the supporting structure moved towards the free face under the active earth pressure of the rear-side soil and the ground surface behind the supporting structure generated settlement. Figure 18 exhibits that the ground surface settlement curve around the foundation pit displays a "spoon" shape; the maximum ground surface settlement occurred at the 1.5 m position behind the supporting structure; the maximum ground surface settlement was −4.08 mm, which is far smaller than the alarm value [31]. In the direction away from the foundation pit, ground surface settlement became increasingly small with increasing distance. The disturbing influence of the foundation pit excavation was when the soil became increasingly small. At the position 6 m away from the supporting structure, ground surface settlement decreased to −0.6 mm, which was small. The ground surface settlement curve had a turning point. Thus, the main influence area of the ground surface settlement, caused by foundation pit excavation, was 0.92 *H*.

Analysis of Settlement Curve Shape

According to the study results of Li [28], the influence area of the soil behind the foundation pit wall was divided as demonstrated in Figure 19, where *L* is the length of the foundation pit.

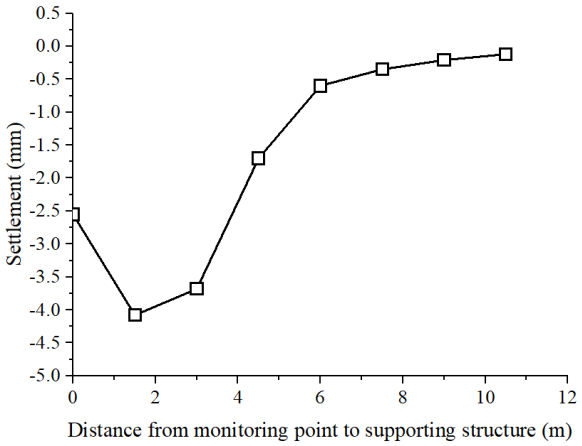

Figure 19. Division of the influence area of the soil behind the foundation pit.

The ground surface settlement patterns in Areas A and B are exhibited in Figure 20.

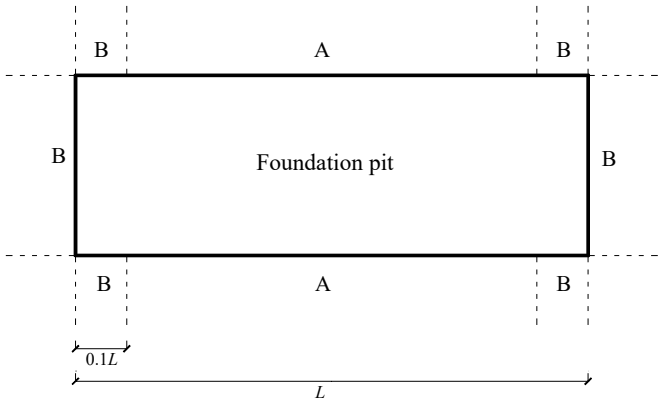

Figure 20. Ground surface settlement curve.

In Figure 20, X_d is the x-coordinate of the maximum settlement point, X_z is the x-coordinate of the turning point of the settlement curve, and X_0 is the x-coordinate of the zero-settlement point in the settlement curve; furthermore, S_z is the ground surface settlement value of the turning point of the settlement curve, S_0 is the ground surface settlement value near the supporting structure, and S_m is the maximum ground surface settlement value. An analysis showed that the two settlement patterns had similar shapes. The maximum ground surface settlement and boundary of the influence area in the ground surface settlement curve were larger in Area A than in Area B. Both settlement curves presented a "square root" shape, different to the ground surface settlement curve shape caused by the foundation pit excavation under the support of recyclable large-diameter steel-pipe piles.

Based on the ground surface settlement patterns proposed by Li [28], a broken line was used to draw the ground surface settlement curve; the result obtained through Li's method [28] was compared to the measured result, as presented in Figure 21.

Based on the observation of the curve plotted in Figure 21, when $X \leq 1.5$ m, the settlement curve is a straight line; the curve proposed by Li [28] agrees with the field test result. When 1.5 m < X < 6 m, a considerable difference exists between the two curves. When 6 m $\leq X \leq$ 10.5 m, the two curves are identical. Therefore, it is necessary to further analyze the shape of the settlement curve generated during the excavation of a foundation pit under the support of recyclable large-diameter steel-pipe piles.

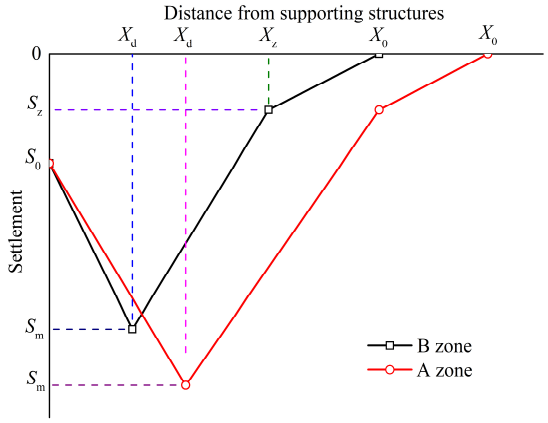

Figure 21. Comparison of the ground surface settlement curve obtained through Li's method and the measured result.

Through further analysis of the settlement curve, it was found that the piecewise function can be used to describe the shape of the settlement curve. The function expressions are shown in Equations (4) and (5).

$$y = ax + b \ (x \leq X_d), \tag{4}$$

$$y = \frac{aX_d + b}{\left[1 + \frac{(x - X_d)^c}{d}\right]} \ (x > X_d), \tag{5}$$

where

y—ground surface settlement value;

x—horizontal coordinate of the ground surface settlement monitoring point;

a, b, c, d—parameters;

X_d—horizontal coordinate of the maximum ground surface settlement monitoring point.

Based on Equations (4) and (5), the nonlinear curve fit method was used to fit the measured settlement data to obtain the fitted settlement curve. The values of the four parameters a, b, c and d are −1.02, −2.55, 3.4, and 34.1 respectively; then, the fitted curve was compared to the measured settlement data and the settlement curve proposed by Li [28], as shown in Figure 22.

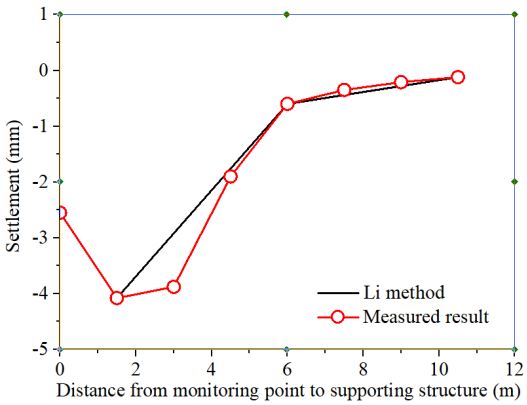

Figure 22. Comparison of the ground surface settlement curves obtained through three methods.

Li [28] approximated the ground surface settlement between the maximum settlement point and the turning point of the settlement curve as a straight line, which has a poor fitting degree with the ground surface settlement curve in the field test result. The proposed piecewise function can depict the ground surface settlement well.

4. Conclusions

The excavation process of the foundation pit supported by large-diameter recyclable steel-pipe piles was analyzed by a field test and the finite element simulation method, and the mechanical performance of the pile was acquired. The following conclusions were drawn from this study:

(1) Upon completing the foundation pit excavation, front- and rear-side strains of the pile body were approximately symmetrical. The value of the pile-body strain was 0 near the undersurface of the foundation pit. The pile body also experienced negative bending at the position above the undersurface of the foundation pit. The maximum pile-body strain occurred at 0.62 H below the ground surface. In addition, the pile body went through positive bending at the position below the undersurface of the foundation pit. The maximum pile-body strain occurred at 0.23 H.

(2) During the foundation pit excavation process, the pile body experienced displacement towards the pit. Pile-top displacement gradually increased with the excavation depth. After the excavation, the pile-top displacement reached the maximum value of 5.63 mm.

(3) The ground surface settlement curve caused by the foundation pit excavation presented a "Spoon" shape. In the direction away from the foundation pit, ground surface settlement initially increased. Then, the tendency decreased with the increase in distance. The maximum ground surface settlement occurred at 0.23 H behind the supporting structure. The main influence area of the ground surface settlement caused by foundation pit excavation was 0.92 H.

(4) The calculation result, obtained through the finite element analysis, showed that the pile-body deformation laws were consistent with the measured ones. The maximum normal stress was 56.9 MPa, which was smaller than the design value of steel flexural strength. Therefore, the pile-body structure was safe.

(5) A suitable mathematical expression of ground surface settlement curve shape was proposed. Through a comparison, the proposed formula can express the shape of the settlement curve well.

(6) Given the condition restriction in this test, the obtained ground surface settlement monitoring data were limited. Therefore, in future work, it is necessary to analyze the parameters of mathematical expressions in the case of more abundant monitoring data.

Author Contributions: Conceptualization, J.L. and Y.L.; methodology, J.L.; software, J.L.; validation, J.L. and Y.L.; formal analysis, J.L.; investigation, J.L., Y.L. and A.Y.; resources, Y.L.; data curation, J.L. and A.Y.; writing—original draft preparation, J.L.; writing—review and editing, Y.L. and A.Y.; visualization, J.L.; supervision, A.Y.; project administration, Y.L.; funding acquisition, Y.L. All authors have read and agreed to the published version of the manuscript.

Funding: This study was supported by the Youth Technology Top Talent Project of RIOH and China Scholarship Council (CSC).

Institutional Review Board Statement: Not applicable.

Informed Consent Statement: Not applicable.

Data Availability Statement: Data will be made available on reasonable request.

Acknowledgments: Thanks for the support from Jinwei Wang, Xiaopeng Kang, and Xiyao Ji.

Conflicts of Interest: The authors declare no conflict of interest.

References

1. Wang, Z.H.; Zhou, J. Three-dimensional numerical simulation and earth pressure analysis on double-row piles with consideration of spatial effects. *J. Zhejiang Univ.-Sci. A Appl. Phys. Eng.* **2011**, *12*, 758–770. [CrossRef]
2. Dong, Y.P.; Burd, H.J.; Houlsby, G.T. Finite-element analysis of a deep excavation case history. *Geotechnique* **2015**, *66*, 1–15. [CrossRef]
3. Goh, A.T.C.; Zhang, F.; Zhang, W.; Zhang, Y.; Liu, H. A simple estimation model for 3D braced excavation wall deflection. *Comput. Geotech.* **2017**, *83*, 106–113. [CrossRef]

4. Zhang, W.; Goh, A.T.C.; Xuan, F. A simple prediction model for wall deflection caused by braced excavation in clays. *Comput. Geotech.* **2015**, *63*, 67–72. [CrossRef]
5. Zhao, Q.J.; Liu, Z.G. Application of recycling anchor cables in support of excavations. *Chin. J. Geotech. Eng.* **2012**, *34*, 480–483.
6. Li, Z.P.; Huang, M.L.; Wang, J. Study on the Recoverable Anchor Cable Supporting Scheme Optimization Design for Metro Foundation pit. *Chin. J. Undergr. Space Eng.* **2012**, *8*, 154–160.
7. Zhang, J.H. Recycling excavation support system (RESS) for foundation pits. *Chin. J. Geotech. Eng.* **2012**, *34*, 287–291.
8. Xiao, T.L.; He, Y.L. Experimental Study of an Inflatable Recyclable Anchor. *Adv. Mater. Sci. Eng.* **2018**, *2018*, 6940531. [CrossRef]
9. Pan, Y.; Fang, H.; Li, B.; Wang, F. Stability analysis and full-scale test of a new recyclable supporting structure for underground ecological granaries. *Eng. Struct.* **2019**, *192*, 205–219. [CrossRef]
10. Li, Z.; Teng, Y.J.; Li, Q.R. Micro-pile techniques for improvement project of existing buildings. *China Civ. Eng. J.* **2015**, *48*, 197–201.
11. Zhang, M.Y.; Li, S.N.; Peng, W.T. Simulation of vertical bearing characteristics of super-long diameter steel pipe piles based on FLAC^{3D}. *Rock Soil Mech.* **2011**, *32*, 2856–2860. (In Chinese) [CrossRef]
12. Liu, Z.S. Field tests on negative skin friction of steel pipe piles in high backfilling soils. *Chin. J. Geotech. Eng.* **2015**, *37*, 337–342. [CrossRef]
13. Wang, M.Y.; Shan, Z.G.; Rao, X.B. Numerical inversion study on comprehensive capacity of marine steel pipe pile based on field pile loading tests. *Chin. J. Geotech. Eng.* **2016**, *38*, 143–148. [CrossRef]
14. Ou, C.Y.; Hsieh, P.G.; Chiou, D.C. Characteristics of ground surface settlement during excavation. *Can. Geotech. J.* **1993**, *30*, 758–767. [CrossRef]
15. Peck, R.B. Deep excavations and tunneling in soft ground. In Proceedings of the 7th International Conference of Soil Mechanics & Foundation Engineering, Mexico City, Mexico, 1969; pp. 225–290. Available online: https://www.scirp.org/reference/referencespapers?referenceid=1768642 (accessed on 28 June 2024).
16. Hsieh, P.G.; Ou, C.Y. Shape of ground surface settlement profiles caused by excavation. *Can. Geotech. J.* **1998**, *35*, 1004–1017. [CrossRef]
17. Wei, G.; Hua, X.X.; Yu, X.F. Construction monitoring analysis of deep foundation pit excavation of a metro station in Hangzhou. *Eng. J. Wuhan Univ.* **2016**, *49*, 917–923. [CrossRef]
18. Goh, A.T.C.; Zhang, R.H.; Wang, W.; Wang, L.; Liu, H.L.; Zhang, W.G. Numerical study of the effects of groundwater drawdown on ground settlement for excavation in residual soils. *Acta Geotech.* **2019**, *15*, 1259–1272. [CrossRef]
19. Zhang, W.; Wang, W.; Zhou, D.; Zhang, R.; Goh, A.T.C.; Hou, Z. Influence of groundwater drawdown on excavation responses—A case history in Bukit Timah granitic residual soils. *J. Rock Mech. Geotech. Eng.* **2018**, *10*, 856–864. [CrossRef]
20. Zhang, W.G.; Goh, A.T.C.; Goh, K.H.; Chew, O.Y.S.; Zhou, D.; Zhang, R. Performance of braced excavation in residual soil with groundwater drawdown. *Undergr. Space* **2018**, *3*, 150–165. [CrossRef]
21. Hong, Y.; Ng, C.; Liu, G.; Liu, T. Three-dimensional deformation behaviour of a multi-propped excavation at a "greenfield" site at Shanghai soft clay. *Tunn. Undergr. Space Technol.* **2015**, *45*, 249–259. [CrossRef]
22. Hsiung, B.-C.B.; Yang, K.-H.; Aila, W.; Hung, C. Three-dimensional effects of a deep excavation on wall deflections in loose to medium dense sands. *Comput. Geotech.* **2016**, *80*, 138–151. [CrossRef]
23. Gong, Y.F.; Yao, A.J.; Li, Y.L.; Li, Y.Y.; Li, Y.N.; Sun, Y.T. Model test study on sliding-toppling composite deformation evolution of anti-dip layered rock slope. *Bull. Eng. Geol. Environ.* **2023**, *82*, 194. [CrossRef]
24. Pakbaz, M.S.; Imanzadeh, S.; Bagherinia, K.H. Characteristics of diaphragm wall lateral deformations and ground surface settlements: Case study in Iran-Ahwaz metro. *Tunn. Undergr. Space Technol.* **2013**, *35*, 109–121. [CrossRef]
25. Li, Y.; Yao, A.; Li, H.; Gong, Y.; Tian, T. Calculation method of multi-stage earth pressure for foundation excavation considering excavation process. *Acta Geotech.* **2023**, *18*, 6123–6141. [CrossRef]
26. Li, Y.-L.; Lu, J.; Yao, A.; Li, H.; Gong, Y.-F. Nonlinear elastic deformation model of belled uplift piles under the coupling effects of groundwater and shear strain relaxation. *Comput. Geotech.* **2024**, *171*, 106411. [CrossRef]
27. Ou, C.-Y.; Shiau, B.-Y.; Wang, I.-W. Three-dimensional deformation behavior of the Taipei National Enterprise Center (TNEC) excavation case history. *Can. Geotech. J.* **2000**, *37*, 438–448. [CrossRef]
28. Li, D.; Li, Z.; Tang, D. Three-dimensional effects on deformation of deep excavations. *Geotech. Eng.* **2015**, *168*, 551–562. [CrossRef]
29. Teo, P.L.; Wong, K.S. Application of the hardening soil model in deep excavation analysis. *IES J. Part A Civ. Struct. Eng.* **2012**, *5*, 152–165. [CrossRef]
30. Chen, Y.M.; Xu, D.P. *FLAC/FLAC3D Foundation and Engineering Example*; China Water & Power Press: Beijing, China, 2013.
31. *GB 50497-2009*; Technical Code for Monitoring of Building Excavation Engineering. China Planning Press: Beijing, China, 2009.